frontiers | Frontiers in Detector Science and Technology

TYPE Original Research
PUBLISHED 05 August 2024
DOI 10.3389/fdest.2024.1438902

OPEN ACCESS

EDITED BY
Piergiorgio Cerello,
National Institute of Nuclear Physics of Turin, Italy

REVIEWED BY
Marco Capogni,
Italian National Agency for New Technologies, Energy and Sustainable Economic Development (ENEA), Italy
Marin Karuza,
University of Rijeka, Croatia

*CORRESPONDENCE
R. Rossini,
riccardo.rossini@infn.it

RECEIVED 26 May 2024
ACCEPTED 02 July 2024
PUBLISHED 05 August 2024

CITATION
Rossini R, Baldazzi G, Banfi S, Baruzzo M, Benocci R, Bertoni R, Bonesini M, Carsi S, Cirrincione D, Clemenza M, Colace L, De Bari A, De Vecchi C, Fasci E, Gaigher R, Gianfrani L, Hillier AD, Ishida K, King PJC, Lord JS, Mazza R, Menegolli A, Mocchiutti E, Monzani S, Moretti L, Petroselli C, Pizzolotto C, Prata MC, Pullia M, Quintieri L, Ramponi R, Rossella M, Sbrizzi A, Toci G, Tortora L, Vallazza ES, Yokoyama K and Vacchi A (2024), The muon beam monitor for the FAMU experiment: design, simulation, test, and operation.
Front. Detect. Sci. Technol 2:1438902.
doi: 10.3389/fdest.2024.1438902

The muon beam monitor for the FAMU experiment: design, simulation, test, and operation

R. Rossini[1,2,3]*, G. Baldazzi[4,5], S. Banfi[6], M. Baruzzo[7], R. Benocci[6,8], R. Bertoni[6], M. Bonesini[6,9], S. Carsi[6,10], D. Cirrincione[7,11], M. Clemenza[6], L. Colace[12,13], A. De Bari[1,2], C. De Vecchi[2], E. Fasci[14,15], R. Gaigher[6], L. Gianfrani[14,15], A. D. Hillier[3], K. Ishida[3,16], P. J. C. King[3], J. S. Lord[3], R. Mazza[6], A. Menegolli[1,2], E. Mocchiutti[7], S. Monzani[7,11], L. Moretti[14,15], C. Petroselli[6,10], C. Pizzolotto[7], M. C. Prata[2], M. Pullia[2,17], L. Quintieri[3], R. Ramponi[18,19], M. Rossella[2], A. Sbrizzi[5], G. Toci[20], L. Tortora[13], E. S. Vallazza[6], K. Yokoyama[3] and A. Vacchi[7,11]

[1]Department of Physics, University of Pavia, Pavia, Italy, [2]Sezione di Pavia, Istituto Nazionale di Fisica Nucleare (INFN), Pavia, Italy, [3]ISIS Neutron and Muon Source, Science and Technology Facilities Council (STFC), Didcot, United Kingdom, [4]Department of Physics "A. Righi", University of Bologna, Bologna, Italy, [5]Sezione di Bologna, Istituto Nazionale di Fisica Nucleare (INFN), Bologna, Italy, [6]Sezione di Milano-Bicocca, Istituto Nazionale di Fisica Nucleare (INFN), Milan, Italy, [7]Sezione di Trieste, Istituto Nazionale di Fisica Nucleare (INFN), Trieste, Italy, [8]Department of Earth and Environmental Sciences (DISAT), University of Milano-Bicocca, Milan, Italy, [9]Department of Physics "G. Occhialini", University of Milano-Bicocca, Milan, Italy, [10]Department of Science and High Technology, University of Insubria, Como, Italy, [11]Department of Mathematics, Computer Science and Physics, University of Udine, Udine, Italy, [12]Department of Engineering, University of Roma Tre, Rome, Italy, [13]Sezione di Roma Tre, Istituto Nazionale di Fisica Nucleare (INFN), Rome, Italy, [14]Department of Mathematics and Physics, University of Campania "Luigi Vanvitelli", Caserta, Italy, [15]Sezione di Napoli, Istituto Nazionale di Fisica Nucleare (INFN), Naples, Italy, [16]RIKEN Nishina Center, Saitama, Japan, [17]Centro Nazionale di Adroterapia Oncologica (CNAO), Pavia, Italy, [18]Sezione di Milano, Istituto Nazionale di Fisica Nucleare (INFN), Milan, Italy, [19]Istituto di Fotonica e Nanotecnologie (IFN), Consiglio Nazionale delle Ricerche (CNR), Milan, Italy, [20]Istituto di Nazionale di Ottica (INO), Consiglio Nazionale delle Ricerche (CNR), Florence, Italy

FAMU is an INFN-led muonic atom physics experiment based at the RIKEN-RAL muon facility at the ISIS Neutron and Muon Source (United Kingdom). The aim of FAMU is to measure the hyperfine splitting in muonic hydrogen to determine the value of the proton Zemach radius with an accuracy better than 1%. The experiment has a scintillating-fibre hodoscope for beam monitoring and data normalisation. In order to carry out muon flux estimation, low-rate measurements were performed to extract the single-muon average deposited charge. Then, detector simulation in Geant4 and FLUKA allowed a thorough understanding of the single-muon response function, which is crucial for determining the muon flux. This work presents the design features of the FAMU beam monitor, along with the simulation and absolute calibration measurements in order to enable flux determination and enable data normalisation.

KEYWORDS

beam monitor, muon, beam calibration, single-particle beam, muonic atom physics, detector simulation

1 Introduction

The aim of the FAMU experiment (Pizzolotto et al. (2020); Vacchi et al. (2023); Rossini et al. (2024a)) is to explore the magnetic structure of the proton through a measurement of the proton Zemach radius (Carlson (2015); Antognini et al. (2022)). The latter is extracted from a measurement of the hyperfine splitting energy of the muonic hydrogen (μH) ground state. μH atoms are produced by injecting a high-rate, low-momentum pulsed muon beam into a pressurised gaseous target. The experiment is currently in operation at the RIKEN-RAL muon facility (Matsuzaki et al. (2001); Hillier et al. (2019)) at the ISIS Neutron and Muon Source (Didcot, UK). The observable of the experiment is the number of delayed muonic oxygen (μO) X-rays resulting from the transfer of the muon from μH to oxygen atoms. This is clearly dependent on the number of μH atoms created, which is directly related to the incoming muon flux. As a consequence, having an accurate and efficient beam monitor with minimal beam absorption is a crucial point in the data normalisation.

A beam hodoscope, composed of two planes of 32 scintillating fibres read out by silicon photomultipliers (SiPMs), has been set up for the experiment. The specific design of this detector, discussed in Section 2, is the best match among the number of available channels (64), the detector area, and its thickness. Other detector designs, such as muon cameras (Lord et al. (2011)), were avoided in order to minimise the amount of material immersed in the beam, as the beam monitor is expected to stay in the beam for the duration of the experiment. Similar detectors for higher rates and continuous beams are being developed at other muon facilities, such as PSI (Papa et al. (2015); Papa et al. (2019); Dal Maso et al. (2023)). The hodoscope serves both as a beam shape detector to optimise beam centring and focussing and as a flux meter. The latter role of the detector is made possible thanks to the analyses reported in this work.

The estimated average negative muon flux with a momentum of 55 MeV/c is on the order of 10^4 muons per second (Matsuzaki et al. (2001); Hillier et al. (2019)). The beam is delivered in two 70-ns spills with an average repetition rate of 40 Hz (the synchrotron rate is 50 Hz, but one in five pulses is directed to the other target station). Therefore, during a spill, approximately 100 muons are delivered in 70 ns. Even though the system is based on a SiPM readout with fast signals (~20 ns), it is clearly not possible to tell single-particle signals apart. For this reason, the detector measures the total deposited charge Q_{tot}, which is converted into muon flux using the result coming from calibration measurements (Carbone et al. (2015); Bonesini et al. (2017); Bonesini et al. (2019); Rossini et al. (2023b); Rossini et al. (2023a); Rossini et al. (2024b)).

Initially, data from cosmic muon calibrations combined with Particle Data Group (PDG) dE/dx results to match the gap between energies of approximately 4 GeV and the used beam momentum (~60 MeV/c), were used to obtain an estimate of the muon flux vs muon beam momentum (Bonesini et al. (2017)), which compared well with previously published results (Matsuzaki et al. (2001)). In this case, two 3-mm pitch hodoscopes (*Hodo-2* and *Hodo-3*) were used.

Then, a 1-mm pitch hodoscope with adjacent fibres (*Hodo-1*) was calibrated at the CNAO synchrotron in Pavia (Italy) with a low-rate proton beam with energy loss dE/dx comparable to FAMU muons (Rossini et al. (2024b)). A proton beam of kinetic energy 150 MeV was tuned to allow single-particle events and directed against the hodoscope for testing.

The latest FAMU hodoscope (*Hodo-4*), that is, the position-sensitive muon beam monitor detector, is here thoroughly discussed. The design of the detector, discussed in Section 2, fits best with the number of available channels (64) and the required thickness, active area, and space resolution. It is composed of 1 mm fibres, spaced by 1 mm. The simulation and tests of the detector are presented in this work. Calibration measurements were carried out in the FAMU setup, exploiting the RIKEN-RAL Port1 muon beam with a modified configuration to obtain a low-rate muon beam, as later explained in Section 3. This has been crucial in order to disclose single-particle signals. In addition, the detector has been simulated in Geant4 (Agostinelli et al. (2003)) and Flair-FLUKA (Battistoni et al. (2015); Ahdida et al. (2022); Vlachoudis (2009)) to understand its response and extract crucial parameters and information for its calibration.

The equation to extract the muon rate from the hodoscope reading is the following:

$$\varphi_\mu = \frac{r}{\left(W_2 + \frac{W_1}{\eta}\right)Q_\mu} Q_{tot} =: kQ_{tot}, \tag{1}$$

where $r = 40$ Hz is the beam repetition rate, Q_{tot} is the total deposited charge during a full-rate beam spill, Q_μ is the average charge deposited by a 55 MeV/c muon interacting with both planes of fibres, Q_μ/η for muons interacting with one fibre only, and $W_{1/2}$ are the fractions of muons interacting with one or two fibres, respectively. The charge deposited in one fibre is written as Q_μ/η because this value is not directly measured, and η is calculated from the simulation. In particular, W_2 is extracted from the simulation, while Q_μ is determined using low-rate data. The main aim of this work, that is, the *calibration* of the FAMU beam monitor, is to compute the value of the calibration factor $k = \frac{r}{(W_2 + W_1/\eta)Q_\mu}$. This work provides a general method to calibrate other fibre-based hodoscopes that will be used as charged particle beam monitors.

Simulation, measurements, and analysis techniques are presented in Sections 3, 4 and 5, whereas the results are extensively presented and discussed in Section 6. Eventually, the value of k is computed, and a test estimation of flux during full-rate beam is shown.

2 Design of the 1-mm hodoscope (Hodo-4)

A 32 × 32 channel (XY configuration) beam monitor has been set up for the FAMU experiment by INFN Milano-Bicocca and INFN Pavia. The hodoscope consists of two crossed planes of 32 single-clad Saint-Gobain/Luxium BCF-12 polystyrene scintillating fibres. Each fibre is squared, with a pitch of 1 mm, and each fibre is covered with a nominal 15 μm-thick layer of TiO_2-based extramural absorber (EMA, or coating) to avoid inter-fibre optical cross-talk.

Previous hodoscope versions (Carbone et al. (2015); Bonesini et al. (2019); Rossini et al. (2023b); Rossini et al. (2023a); Rossini et al. (2024b)) had either too much material immersed in the beam (32 × 32 fibres with a 3 mm pitch, that is, active area of 9.6 × 9.6 cm^2 and a total thickness of 6 mm) or too small active area (32 × 32 fibres

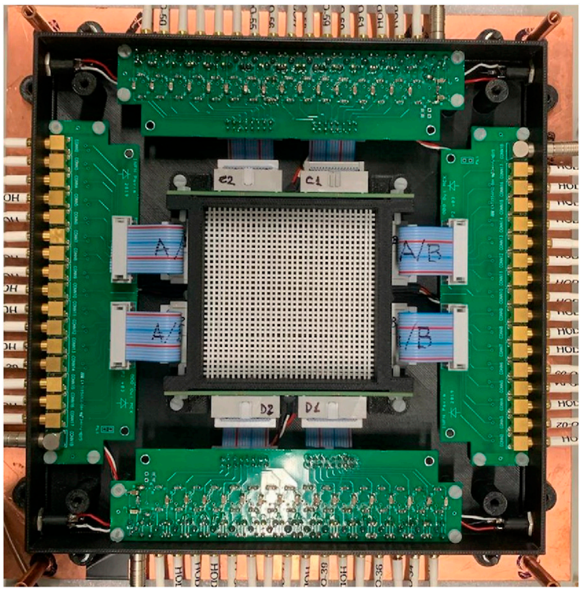

FIGURE 1
Hodoscope without its cover. The interspaced scintillating fibres are clearly visible in the middle (white). The internal printed circuit boards hold the SiPMs, and they are connected by stripes to the external ones, holding the 64 micro coaxial connectors (MCXs, signals) and 4 LEMO (bias supply) connectors.

TABLE 1 Comparison among the various models of 32 × 32 hodoscope developed for the FAMU experiment. Hodoscopes with 1-mm fibres have only a 2 mm thickness but a small active area, whereas those with 3-mm fibres have a larger area but are 6 mm thick. The model described in this work and finally installed in FAMU has 1-mm fibres interspaced by 1 mm, allowing a mid-size active area without compromising the detector thickness.

Hodoscope	Fibre pitch	Thickness	Active area
Hodo-1	1 mm	2 mm	3.2×3.2 cm^2
Hodo-2/3	3 mm	6 mm	9.6×9.6 cm^2
Hodo-4	1 mm	0–2 mm	6.4×6.4 cm^2

with 1-mm pitch, that is, active area of 3.2×3.2 cm^2 and a total thickness of 2 mm). The key point of the detector described in this work is having a spacing of 1 mm between adjacent fibres, as shown in Figure 1. This allows a 6.4×6.4 cm^2 detector area despite keeping the thickness below 2 mm. However, this hodoscope has inhomogeneous volume, which slightly complicates its response function to the muon beam, as further discussed in Sections 5 and 4. In fact, each muon can interact with zero, one, or two fibres depending on its interaction position in the XY plane. The geometric features of this model compared to the previous ones are presented in Table 1.

This model of the hodoscope has been considered the best compromise among all features, and it has, therefore, been installed in the final FAMU setup for 2023 and 2024 runs. Consequently, carrying out single-particle calibration was crucial for its operation in the FAMU experiment. The position of the hodoscope in the FAMU setup is shown in Figure 2.

Each fibre is read out by a 1×1 mm^2 Hamamatsu S12571-050P SiPM (cell size 50 μm) on one side. SiPMs are supplied with a positive bias of 66.64 ± 0.12 V (finely tuned for each group of 16 SiPMs to optimise the uniformity of the detector response)[1]. SiPM signals are fanned out through 4 m cables with MCX connectors and digitised using two CAEN V1742 (32 channels each). The trigger is supplied to all digitisers (including these) through the FAMU system, which provides a beam trigger coming from the synchrotron with a rate of 50 Hz.

3 Hodoscope measurements at RIKEN-RAL Port1

The FAMU experiment is installed at the RIKEN-RAL Port1 muon beamline at the ISIS Neutron and Muon Source in Didcot, United Kingdom. The experiment consists of a pressurised cryostat holding ~ 7.5 bar of a hydrogen-oxygen mixture at a temperature of approximately 90 K. The gas chamber is the target of the muon beam, with the aim of forming muonic hydrogen atoms.

The ISIS synchrotron accelerates protons with an energy of 800 MeV with a pulse rate of 50 Hz. Four consecutive pulses are sent to Target Station 1 (TS1), and one is sent to Target Station 2 (TS2). The graphite target for muon beamlines is located in the beampipe connecting the synchrotron to TS1. Hence, it receives protons and produces muon pulses at the same rate as TS1 ($r = 40$ pulses per second). Negative pions are directed in the RIKEN beampipe, where they decay to negative muons and are delivered to the four RIKEN-RAL Ports alternatively. RIKEN-RAL Port1 is currently dedicated to the FAMU experiment. The beam time structure, which is the same for high and low-rate measurements, is shown in Figure 3 as measured by the FAMU hodoscope in a low-rate test beam. Each beam pulse consists of two 70 ns spills separated by 320 ns.

3.1 High-rate measurements at RIKEN-RAL

The beam is generally set to work at the highest available rate. At the momentum value used in FAMU, the average rate is the order of 10^4 muons/s. The quadrupole and bending magnet configuration have been optimised to deliver the best beam rate and geometry that suit the experiment during the FAMU beam commissioning in July 2023 (4 beam days, dataset *RAL202303*).

After that, two FAMU data-taking runs were carried out in October 2023 (6 beam days, *RAL202305*) and December 2023 (12 beam days, *RAL202306*).

3.2 Low-rate measurements at RIKEN-RAL

After carrying out some tests with protons at the CNAO synchrotron in Pavia (Rossini et al. (2024b)), it was decided to

1 the operational voltage values for the three printed circuit boards (each one holding 16 SiPMs) are as follows: 66.45 ± 0.03 V, 66.65 ± 0.01 V, 66.69 ± 0.01 V, and 66.78 ± 0.02 V.

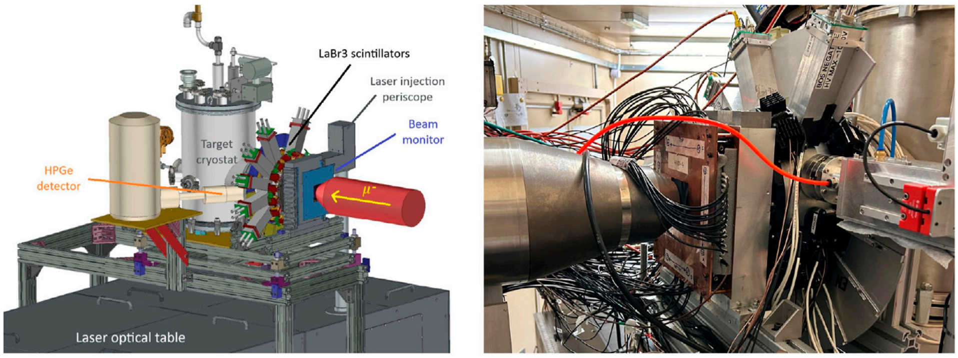

FIGURE 2
FAMU in the 2023 setup. The picture on the left shows a CAD scheme of the target and detector system in the 2023 setup: the hodoscope (beam monitor) is positioned just after the muon beamline collimator, whereas all other detectors ($LaBr_3$ and HPGe) are positioned around the gas target. On the right is shown a picture of the setup, where the hodoscope (copper-shielded detector) is in a close-up view. Figures taken from Rossini et al. (2024b).

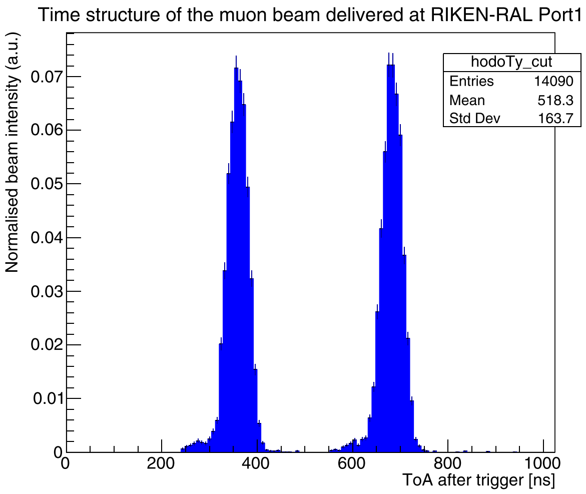

FIGURE 3
Time structure of the muon beam for each trigger. This normalised histogram has been measured by the FAMU hodoscope at a low rate, but the time structure holds for a high rate as well.

characterise the current hodoscope directly on the FAMU setup as its particular design was expected to be more sensitive to beam geometry changes.

In order to obtain a single-particle beam, the currents of some quadrupole and bending magnets were de-tuned to minimise the amount of pions directed in the beampipe. In particular, the first two quadrupoles (RQ1 and RQ2) were turned off to widen the pion bunch, and the first bending magnet (RB1) was de-tuned to direct the beam halo, rather than its central part, into the beampipe. See Figure 4 for a detailed map of the path followed by the beam from the target to Port1, including the magnets encountered. The choice of which magnets had to be tuned was made to not compromise the beam optics, which would result in not delivering the beam to Port1. The shut-down of the two quadrupoles resulted in a ~90% beam intensity drop. The optimisation of the bending magnet current was carried out progressively to make sure that the rate would be as low as required. Figure 5 shows the effect of the progressive variation of the RB1 current out of its optimal value. The muon current (proportional to Q_{tot}) decreases, whereas the number of events marked as single coincidences increases, reaches a maximum, and starts to decrease. This latter behaviour means that the muon flux is so low it allows events with only one coincidence, that is, single-muon spills.

The low-rate data acquisition *RAL202306* consisted of several hours of beam optimisation and final $50k$-event measurements with and without the beam.

4 Data analysis

The data analysis technique, described in Figure 6, is based on imposing single coincidences between each detector plane.

For each beam trigger, the FAMU DAQ system opens an acquisition window and digitises the signals coming from each hodoscope channel at a rate of 1 G/s. The resulting data packet is called an event. In the previous analysis procedure, extensively described and tested by Rossini et al. (2024b), an event was considered a single-particle hit if only one fibre per plane had integrated charge over a given threshold. This method has been considered valid as the hodoscopes had no interspacing, and the measurements were particle-triggered. This means that most muons arrived at the same time (given the fixed pre-trigger window) and passed by one fibre per plane. However, in this case, the trigger comes from the synchrotron, and the full-rate beam shape is complex (every synchrotron trigger corresponds to two ~70 ns spills separated by a ~320 ns gap). The low-rate time structure of the beam is the same: even though the beam is tuned to allow single-particle events, they might come from either the first or the second spill, and some events might have more than one muon. In addition, the spacing between adjacent fibres makes it less probable to have muons hitting one fibre per plane, as better discussed and quantified in Section 5. For this reason, it was decided to use a time coincidence-based approach.

During data processing, for each event and for each hodoscope fibre j, the hodoscope low-rate data processing system retrieves the 64 waveforms and looks for peaks, returning the total integrated charge Q_j and, for every peak k, the time-of-arrival t_j^k and the pulse height PH_j^k. At this point, the coincidence is imposed, with a tolerance of 50 ns (small enough to exclude particles coming from two different

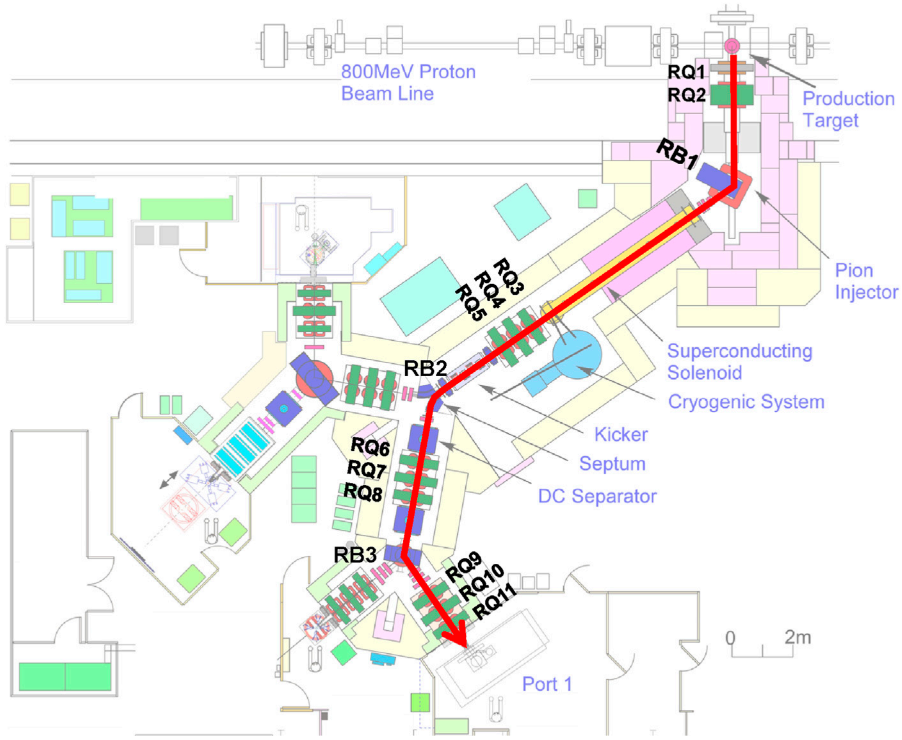

FIGURE 4
Path followed by the negative muons (red arrow) from the graphite target to Port1, where the FAMU target and detectors are located. The quadrupole (RQ) and bending magnets (RB) implied in the delivery of muons to FAMU are labelled. Adapted from https://www.isis.stfc.ac.uk/.

spills), for hodoscope peaks having PH_j^k over a certain threshold to be determined. Events with only one coincidence are selected as single-particle events and used for the hodoscope characterisation.

The value of total deposited energy for every event is the sum on all fibres of the integrated charge $Q_{tot} = \sum_{j=1}^{64} Q_j$. This holds for both low- and high-rate measurements. As one can see in Section 6, the shape of the Q_{tot} histogram for low-rate measurements is asymmetric. After exploring some possibilities (combinations of Landau and Gauss profiles), it has been decided to fit this histogram with the convolution of a Gaussian and a decreasing exponential profile; that is:

$$\begin{aligned} F(x) &= A\int_{-\infty}^{x} dt\ e^{-t/\tau}\ G_{\mu,\sigma}(x-t) \\ &= C + A\exp\left[-\frac{x-\mu}{\tau} + \frac{\sigma^2}{2\tau^2}\right]\left(1 + \mathrm{erf}\left(\frac{x-\mu-\sigma^2/\tau}{\sqrt{2}\,\sigma}\right)\right), \end{aligned} \tag{2}$$

having five free parameters: additive constant C, amplitude A, Gaussian mean μ, Gaussian sigma σ, and exponential decay constant τ. The fit boundaries are chosen by looking for optimal and stable reduced χ^2. The maximum, which corresponds to the estimate for Q_μ, has no known analytical expression. Consequently, it was determined on the fit function through the numerical Brent method[2]. The uncertainty on Q_μ is obtained by variations of the fit boundaries around the optimum. This is done recursively to select a region in the two fitting boundaries in which $\chi^2/NDF < 1.3$. The variation of Q_μ in this region is then used as an estimation for its uncertainty.

The value obtained by analysing the data taken at RIKEN-RAL with low-rate muons is $Q_\mu = (13220 \pm 40)$ ADC channels. The uncertainty is taken by varying the fitting boundaries and imposing $\chi^2/NDF < 1.3$. The histogram and fit are shown in Figure 7. This is the most probable value of deposited charge by 55 MeV/c muons interacting with two scintillating fibres, one per plane. As discussed, the muon flux with this geometry cannot be simply obtained as Q_{tot}/Q_μ, as most muons do not interact with two fibres. However, the fraction of muons interacting with one fibre per plane (W_2) and with one fibre only (W_1) is mostly geometric and must be extracted from the simulation. Therefore, the flux can be estimated with Eq. 1, that is, weighting Q_{tot}/Q_μ by a factor $1/(W_2 + W_1/\eta)$, which is obtained from the simulation in Section 5.

5 Hodoscope simulation

In order to understand the energy loss of muons in the detector and, therefore, its theoretical response function, the hodoscope has been simulated using the Geant4 (Agostinelli et al. (2003)) toolkit. The geometry consists of the fibres, coatings and entrance windows as described in Section 2; that is, each fibre (polystyrene, 1 mm pitch, 6.4 cm length) is coated with a 15 μm layer of TiO_2 and positioned in a 32-fibre plane with 1 mm interspacing between adjacent fibres (measured coating-to-coating); two planes are juxtaposed with crossing fibre direction, separated from the world volume with a 0.1-mm-thick PVC window.

2 Using the ROOT (Brun and Rademakers (1997) method TF1: GetMaximumX.

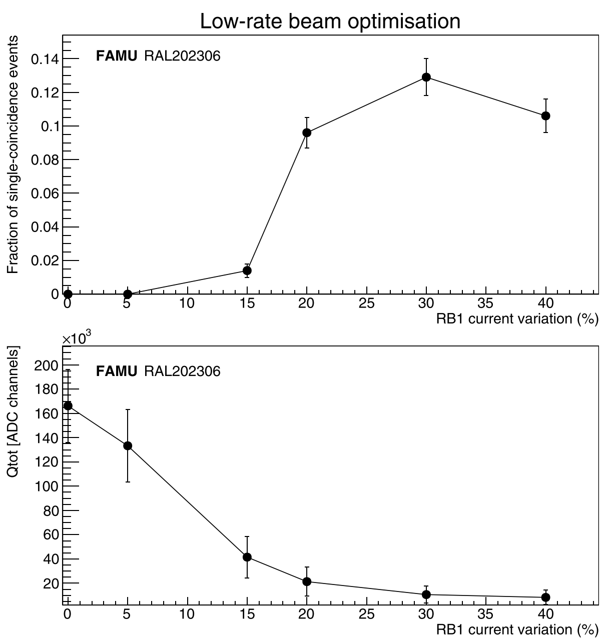

FIGURE 5
Optimisation of the RB1 current to obtain the low-rate configuration. The upper panel shows the fraction of events selected as single-particle events as a function of the RB1 current displacement, while the lower one shows the related decrease of Q_{tot}. Working at RB1+40% guarantees low-rate conditions.

The muon beam simulated for this work is a 55 MeV/c negative muon beam with 2-dimensional Gaussian shape, with $\sigma_X = (8.15 \pm 0.02)$ mm and $\sigma_Y = (10.354 \pm 0.012)$ mm. The reproduces the beam configuration optimised for the experiment, as measured with the hodoscope during 12 h of full-rate data acquisition.

In order to obtain an uncertainty budget, all simulations were repeated with Gaussian dispersion of momentum ($\sigma_p/p = 10\%$), variable beam size within the σ_X-σ_Y uncertainties, and variable coating thickness, considering a 5 μm coating thickness tolerance. This resulted in a geometric systematic uncertainty, which was added to the uncertainty budget as an independent contribution.

All primaries have been tracked and assigned flags depending on whether they passed by front and back plane fibres. In fact, given the geometry of the hodoscope, muons can pass by zero, one, or two fibres. The contributions of these muons are plotted separately and also jointly in Figure 8. In the zero-hit case, the energy deposit different from zero in some events is caused by secondary particles (*e.g.*, delta rays generated in the coating and decay electrons) interacting with the fibres. The probability of hitting zero, one, or two fibres is about 25%, 50%, and 25%, respectively, as one can derive from geometrical considerations from Figure 9. However, the exact values of W_2 and W_1 depend on beam geometry, scattering processes, and coating thickness; as a consequence, they must be extracted from the simulation. W_1 is equal to the fraction of particles interacting with only one fibre, while W_2 is the fraction of muons passing by two fibres, one per plane.

In the Geant4 simulation, 10^6 negative muons with momentum 55 MeV/c were launched. The beam geometry is the one extracted from 12 h of full-rate hodoscope measurements. As expected, about $\frac{1}{4}$ of the muons were marked as passing by two fibres, with a statistical counting uncertainty of around 0.2%. The uncertainty budget was completed by repeating the simulation with variations in the fibre pitch within its tolerance (30 μm), the coating thickness within 5 μm, the beam momentum within 10%, and the beam shape within the measured uncertainty. Other effects, such as small fibre misplacements, are expected to be averaged and cancelled due to the beam spot size. The total contribution, which is dominated by the uncertainty on the coating thickness, is about 1.8% on the number of muons passing by two fibres. The final estimate for the double-hit fraction is $W_2 = (24.9 \pm 0.4)\%$. This value is consistent with the heuristic value of 25% estimated from the geometry of the detector elementary cells. Similarly, the single-hit fraction estimate is $W_1 = (49.61 \pm 0.09)\%$.

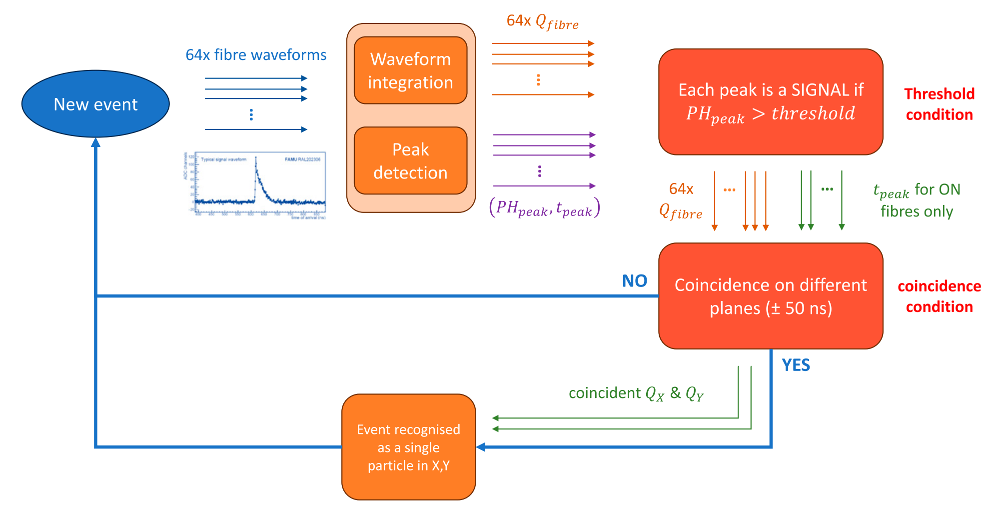

FIGURE 6
Scheme of the coincidence data processing workflow, described in Section 4, to select events with a single muon interacting with both detector planes (*2-hit* data).

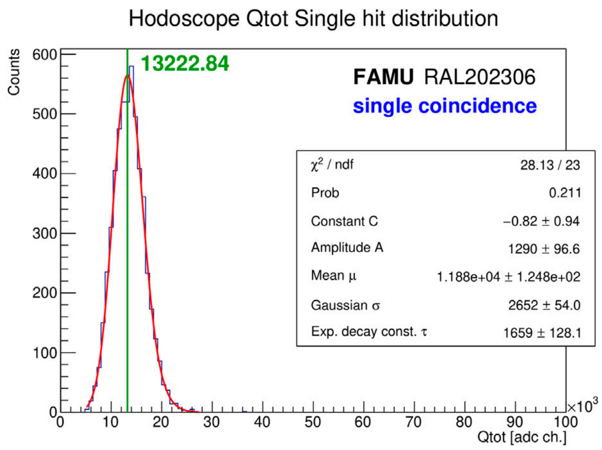

FIGURE 7
Determination of Q_{μ} from the fit of the low-rate Q_{tot} histogram. The fitting function is the distribution in Eq. 2, and the maximum is obtained with the numerical Brent method.

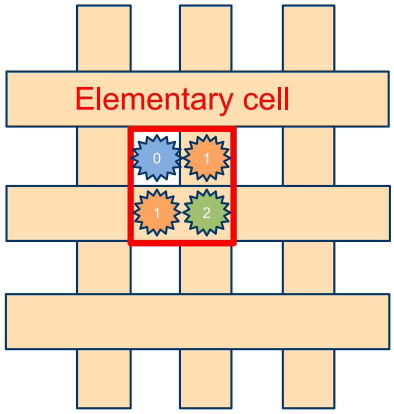

FIGURE 9
Graphical representation of the hodoscope subdivision in elementary cells (red). As one can derive from the scheme, assuming uniform flux, muons can interact with either zero (blue), one (orange), or two fibres (green) with probabilities of ~ 25%, 50%, and 25%, respectively. As a consequence, the heuristic values to be compared to the simulation are W_2 ~ 0.25 and W_1 ~ 0.5.

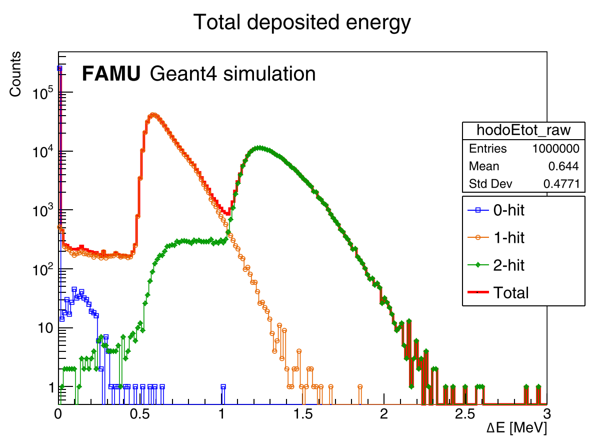

FIGURE 8
Geant4 simulation (10^6 events): energy deposited in scintillating fibres by muons interacting with zero (blue squares), one (orange circles), and two (green diamonds) fibres. The total contribution (thick red line) is the expected response function of the detector.

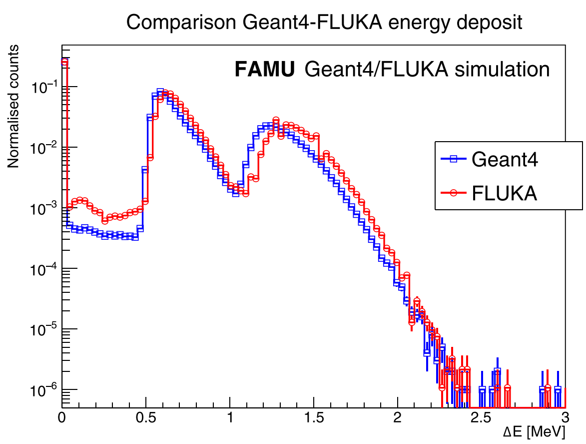

FIGURE 10
Comparison of Geant4 (blue squares) and FLUKA (red circles) simulated energy deposited in hodoscope fibres (10^6 events). The two energy peaks differ by 6%–7%, which is considered good qualitative accordance between the two approaches. Fine differences between the spectra are currently being investigated.

In addition, the ratio η between the double-hit and the single-hit mean deposited energy had to be computed. In fact, the data selection described in Section 4 enables only the inclusion of double-hit events. As a consequence, the value of Q_{μ} calculated from the measurements is only the mean charge deposited by particles hitting two fibres. In principle, with a local linear approximation of the energy-loss curve, one could assume that the energy released by single-hitting muons is $Q_{\mu}/2$ (*i.e.*, that $\eta = 2$, but this must be verified, as the linear approximation might not hold. To do so, the single- and double-hit simulated spectra (see Figure 8) were fitted with Eq. 2. The fit stability was tested and used to determine the uncertainties as in the case of data coming from low-rate measurements (see Section 4), along with parameter variation. The estimated values of deposited energy are $E_2 = (1.23 \pm 0.06)$ MeV for the 2-hit and $E_1 = (0.58 \pm 0.03)$ MeV for the 1-hit. The resulting beam momentum straggling, which comes from the sparse detector geometry, is comparable to the momentum bite of the incoming beam (dp/p ~ 4% (Matsuzaki et al. (2001))) and small compared to the stopping range in the FAMU apparatus. As a consequence, the presence of the hodoscope does not spoil the FAMU data.

The estimate for the ratio between the double-hit and the single-hit mean deposited energy is $\eta = E_2/E_1 = 2.11 \pm 0.05$.

In parallel, an independent simulation based on the FLUKA-CERN (Battistoni et al. (2015); Ahdida et al. (2022)) toolkit was also developed using the Flair interface (Vlachoudis (2009)) for comparison (reported just as FLUKA in this work, for

TABLE 2 Comparison between parameters estimated by the Geant4 and FLUKA simulations with 10^6 events simulated. The uncertainty balances are obtained through parameter variation, whereas those marked with “stat” are statistical only. The values of W_2 are consistent with each other, while the values of W_1 are qualitatively comparable and differ by less than three standard deviations (Student’s t-test). The estimates of E_2, E_1, and η are consistent between the two independent simulation toolkits.

Toolkit	W_2	W_1	E_2 (MeV)	E_1 (MeV)	$\eta = E_2/E_1$
Geant4	24.9 ± 0.4	49.61 ± 0.09	1.23 ± 0.06	0.58 ± 0.03	2.11 ± 0.05
FLUKA	$25.17 \pm (0.06)_{stat}$	$49.94 \pm (0.07)_{stat}$	1.32 ± 0.03	0.62 ± 0.02	2.13 ± 0.08

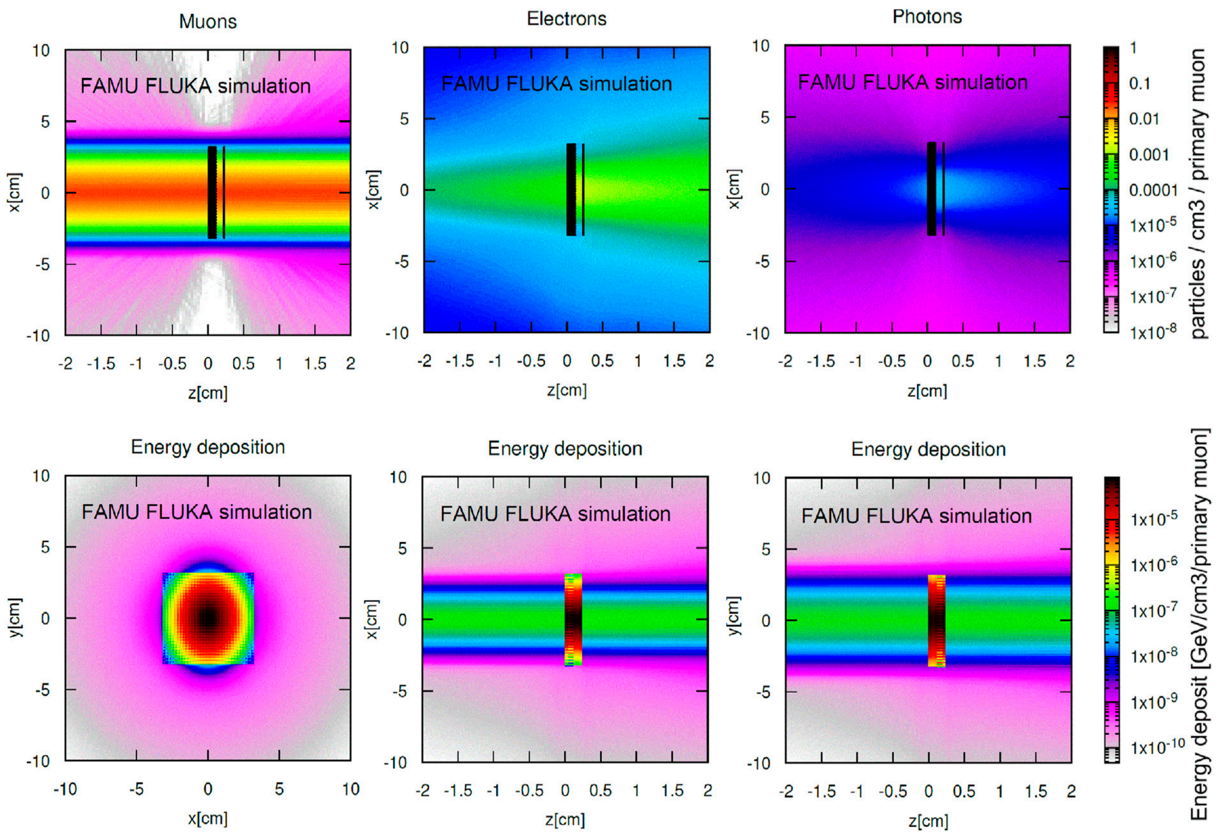

FIGURE 11
2D distributions extracted from the Flair interface to the FLUKA simulation. The muon beam runs along the z axis in the positive direction (left to right). The first row shows the density of muons/electrons/photons in the path followed by the muons, with the same colour scale for all plots. The second row shows the spatial distribution of the energy deposit.

simplicity). The FLUKA simulation has been modelled to match the exact geometry and beam characteristics with the one in Geant4. The geometric factors determined with the FLUKA simulation with the same number of events (10^6) are: $W_2^{\mathrm{FLUKA}} = (25.17 \pm 0.06)\%$ and $W_1^{\mathrm{FLUKA}} = (49.94 \pm 0.07)\%$. The uncertainties on the FLUKA predictions are underestimated as they only comprise the statistical component. Both values differ by less than three standard deviations from the values estimated in Geant4. The qualitative comparison between the FLUKA and Geant4 histograms of the energy deposited in the hodoscope active volumes is shown in Figure 10. The deposited energies in the 1-hit and 2-hit cases, obtained from fitting with Eq. 2, are $E_2^{\mathrm{FLUKA}} = (1.32 \pm 0.03)$ MeV and $E_1^{\mathrm{FLUKA}} = (0.62 \pm 0.02)$ MeV. These energy deposits differ by about 7% and 6%, respectively, from the Geant4 values. Such a difference is generally considered a sign of accordance between the results retrieved from two independent codes. Their ratio is $\eta^{\mathrm{FLUKA}} = 2.13 \pm 0.08$, which is consistent with the value extracted from the Geant4 simulation.

The FLUKA simulation was also used to estimate effective backscattering, that is, the fraction of particles interacting with one fibre in the first plane, one in the second plane, and then one back in the first plane, as a result of backscattering. Ideally, this value should be minimal for better hodoscope accuracy. The effective backscattering rate is (0.013 ± 0.004) ‰, which is negligible.

All the useful parameters extracted from Geant4 and FLUKA simulations are reported in Table 2. The coefficients for Eq. 1 used in this work for flux estimation are taken from the Geant4 simulation because the applied physics lists and transport thresholds had already been tuned and validated for the FAMU experiment.

Figure 11 shows some 2D distributions obtained using the Flair interface to FLUKA-CERN. In particular, the first row

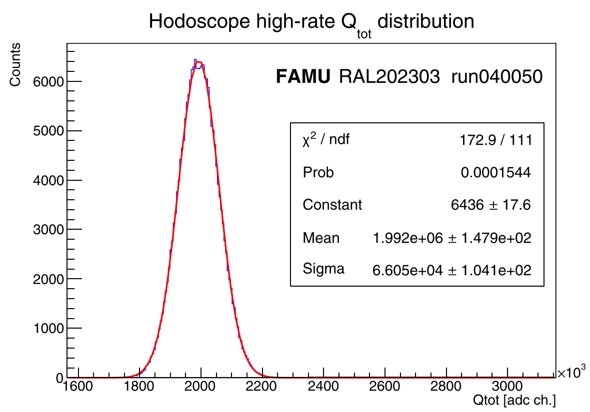

FIGURE 12
Extraction of average Q_{tot} from the fit of a high-rate Q_{tot} histogram with a Gauss profile.

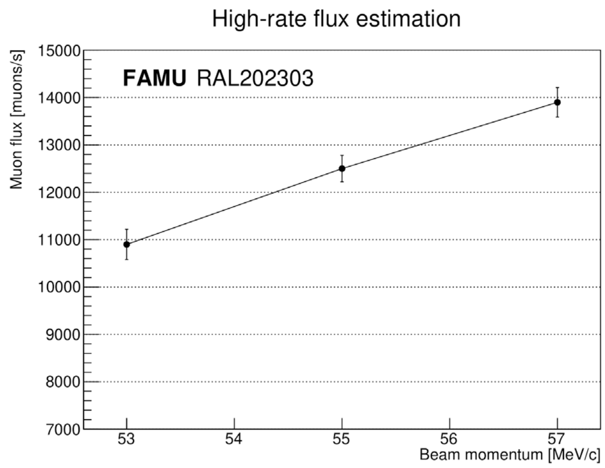

FIGURE 13
Estimation of muon flux from three values of beam momentum. The correction factor for the value of Q_μ is extracted from the simulation.

shows the probability density for the particles present in the simulation (primary muons, decay electrons, and photons/ electrons resulting from elastic and inelastic processes). The second row shows the space distribution of the energy deposition, which is higher in the detector fibres than in air, reflecting the Gaussian shape of the beam on the xy plane. Muon inelastic processes are negligible for the sake of the experiment. The main mechanism of muon energy loss is by delta ray emission and elastic scattering processes.

6 Results

Following the procedures explained in the previous sections of this work, it has been possible to estimate the values of $Q_\mu = (13220 \pm 40)$ ADC channels, $W_2 = (24.9 \pm 0.4)\%$, $W_1 = (49.61 \pm 0.09)\%$, and $\eta = E_2/E_1 = 2.11 \pm 0.05$. The values of W_1, W_2 and η are extracted from the Geant4 simulation as it has already been optimised for muons in this energy range. The physics in the FLUKA simulation is currently being tuned, but the first results presented in Section 5 are qualitatively promising. Hence, the value of the calibration factor k in Eq. 1 is

$$k = (6.25 \pm 0.15) \cdot 10^{-3} \, (\mathrm{s} \cdot \mathrm{ADC\,ch.})^{-1}. \tag{3}$$

Fitting the full-rate beam histogram of the charge deposited in the hodoscope in each muon spill with a Gaussian profile (see Figure 12) made it possible to extract the average value of Q_{tot} for the analysed run. However, this flux estimation can also be carried out event-by-event simply taking the punctual value of Q_{tot} and converting it into punctual muon flux. Taking the mean value and converting it into mean muon rate by applying Eq. 1 with the value of k in Eq. 3, one gets $(1.25 \pm 0.03) \cdot 10^4$ muons/s. This value has been obtained with synchrotron current ~ 85% the maximum value. It is consistent with the expected order of magnitude for the 55 MeV/c negative muon flux at full synchrotron current ($>10^4$ muons/s) (Matsuzaki et al. (2001); Hillier et al. (2019)).

By extracting weighing factors for Q_μ at other momenta from the simulation, it has also been possible to estimate the muon flux during high-rate measurements at momentum different from 55 MeV/c. The result is presented in Figure 13, and the trend is increasing with momentum, as expected.

7 Conclusion

A full calibration protocol for a beam hodoscope that will be used as a flux monitor has been explained, applied, and tested.

When the beam repetition rate r is known, the values of W_2 W_1, and η are extracted from simulation, and the value of Q_μ is extracted from low-rate measurements allowing single-particle events. In particular, by modelling the detector in a simulation toolkit (Geant4/FLUKA), W_2 and W_1 are obtained by counting the primary muons interacting with fibres in both planes of the detector or with one fibre only, respectively, whereas η is the ratio of the mean deposited energies in the two cases. On the other hand, Q_μ is obtained by tuning the beampipe (bending and quadrupole) magnets to deliver a small fraction of the beam. By tuning the magnets to allow single-particle spills to reach the detector, it was possible to determine the amount of charge deposited by muons hitting two fibres by imposing coincidence between the two planes during data analysis. This allowed to calculate the calibration constant k to convert the high-rate deposited charge Q_{tot} into the muon rate φ_μ. The muon rate plays a crucial role in the data normalisation for the FAMU experiment.

This protocol can be applied to similar detectors to use them for the same particle counting task in cases where single-particle discrimination is not possible.

This procedure can be carried out with any scintillating fibre-based hodoscope that will be used as a muon beamline monitor with various applications. For example, muonic atom X-ray spectroscopy (μ-XES), used for elemental and isotopic analysis (Clemenza et al.

(2019); Cataldo et al. (2022); Rossini et al. (2023c)), is a non-destructive technique for the depth-dependent characterisation of materials of interest such as Cultural Heritage samples. It consists of a spectroscopic analysis of the muonic atom X-rays emitted by a sample. Hence, knowing the injected beam rate would give important information about the number of atoms created, helping quantify the elements and isotopes present in the sample. The presence of a calibrated beam hodoscope in such applications would, therefore, help improve the technique.

Data availability statement

The raw data supporting the conclusions of this article will be made available by the authors, without undue reservation.

Author contributions

RRo: conceptualization, data curation, formal analysis, investigation, methodology, resources, software, supervision, validation, visualization, writing–original draft, and writing–review and editing. GB: methodology, resources, and writing–review and editing. SB: resources and writing–review and editing. MB: resources and writing–review and editing. RBn: resources and writing–review and editing. RBr: resources and writing–review and editing. MB: resources, writing–review and editing, funding acquisition, investigation, and supervision. SC: resources and writing–review and editing. DC: resources and writing–review and editing. MC: resources and writing–review and editing. LC: resources and writing–review and editing. AD: resources and writing–review and editing. CD: resources and writing–review and editing. EF: resources and writing–review and editing. RG: resources and writing–review and editing. LG: resources and writing–review and editing. AH: investigation, methodology, resources, writing–review and editing, and supervision. KI: resources, writing–review and editing, investigation, and methodology. PK: resources and writing–review and editing. JL: resources, writing–review and editing, investigation, methodology, and validation. RM: resources and writing–review and editing. AM: conceptualization, investigation, methodology, resources, supervision, writing–review and editing, validation, and visualization. EM: resources, writing–review and editing, conceptualization, data curation, investigation, methodology, project administration, software, and supervision. SM: resources and writing–review and editing. LM: resources and writing–review and editing. CPe: resources, writing–review and editing, and validation. CPi: resources, writing–review and editing, funding acquisition, project administration, software, and supervision. MPr: resources and writing–review and editing. MPu: resources and writing–review and editing. LQ: resources, writing–review and editing, formal analysis, investigation, methodology, and software. RRa: resources and writing–review and editing. MR: resources and writing–review and editing. AS: resources, writing–review and editing, software, and supervision. GT: resources and writing–review and editing. LT: resources and writing–review and editing. EV: resources, writing–review and editing, and software. KY: resources and writing–review and editing. AV: conceptualization, funding acquisition, investigation, project administration, resources, supervision, and writing–review and editing.

Funding

The author(s) declare that financial support was received for the research, authorship, and/or publication of this article. The National Scientific Commission 3 (CSN3) of Istituto Nazionale di Fisica Nucleare (INFN) is gratefully acknowledged as the funding agency of the FAMU experiment. The Science and Technology Facilities Council (STFC) is gratefully acknowledged for the beamtime at the ISIS Neutron and Muon Source for the FAMU experiment (beamtime reference number RB2000022). Computing resources were provided by INFN CNAF Tier1 (data analysis and Geant4 simulation) and the STFC Scientific Computing Department's SCARF cluster (FLUKA simulation).

Conflict of interest

The authors declare that the research was conducted in the absence of any commercial or financial relationships that could be construed as a potential conflict of interest.

The author(s) declared that they were an editorial board member of Frontiers, at the time of submission. This had no impact on the peer review process and the final decision.

Publisher's note

References

Agostinelli, S., Allison, J., Amako, K., Apostolakis, J., Araujo, H., Arce, P., et al. (2003). Geant4—a simulation toolkit. *Nucl. Instrum. Methods Phys. Res. Sect. A Accel. Spectrom. Detect. Assoc. Equip.* 506, 250–303. doi:10.1016/s0168-9002(03)01368-81016/S0168-9002(03)01368-8

Ahdida, C., Bozzato, D., Calzolari, D., Cerutti, F., Charitonidis, N., Cimmino, A., et al. (2022). New capabilities of the fluka multi-purpose code. *Front. Phys.* 9, 788253. doi:10.3389/fphy.2021.788253

Antognini, A., Hagelstein, F., and Pascalutsa, V. (2022). The proton structure in and out of muonic hydrogen. *Annu. Rev. Nucl. Part. Sci.* 72, 389–418. doi:10.1146/annurev-nucl-101920-024709annurev-nucl-101920-024709

Battistoni, G., Boehlen, T., Cerutti, F., Chin, P. W., Esposito, L. S., Fassò, A., et al. (2015). Overview of the fluka code. *Ann. Nucl. Energy* 82, 10–18. doi:10.1016/j.anucene.2014.11.007

Bonesini, M., Benocci, R., Bertoni, R., Mazza, R., deBari, A., Menegolli, A., et al. (2019). The upgraded beam monitor system of the famu experiment at riken–ral. *Nucl.*

Instrum. Methods Phys. Res. Sect. A Accel. Spectrom. Detect. Assoc. Equip. 936, 592–594. doi:10.1016/j.nima.2018.08.092092

Bonesini, M., Bertoni, R., Chignoli, F., Mazza, R., Cervi, T., de Bari, A., et al. (2017). The construction of the fiber-sipm beam monitor system of the r484 and r582 experiments at the riken-ral muon facility. *J. Instrum. (JINST)* 12, C03035. doi:10.1088/1748-0221/12/03/c030351748-0221/12/03/C03035

Brun, R., and Rademakers, F. (1997). Root — an object oriented data analysis framework. *Nucl. Instrum. Methods Phys. Res. Sect. A Accel. Spectrom. Detect. Assoc. Equip.* 389, 81–86. doi:10.1016/s0168-9002(97)00048-x1016/S0168-9002(97)00048-X

Carbone, R., Bonesini, M., Bertoni, R., Mazza, R., Rossella, M., Tortora, L., et al. (2015). The fiber-sipmt beam monitor of the r484 experiment at the riken-ral muon facility. *J. Instrum. (JINST)* 10, C03007. doi:10.1088/1748-0221/10/03/C03007

Carlson, C. (2015). The proton radius puzzle. *Prog. Part. Nucl. Phys.* 82, 59–77. doi:10.1016/j.ppnp.2015.01.002

Cataldo, M., Clemenza, M., Ishida, K., and Hillier, A. (2022). A no*vel non*-destructive technique for cultural heritage: depth profiling and elemental analysis underneath the surface with negative muons. *Appl. Sci.* 12, 4237. doi:10.3390/app12094237app12094237

Clemenza, M., Baldazzi, G., Ballerini, G., Bonesini, M., Carpinelli, M., Cremonesi, O., et al. (2019). Chnet-tandem experiment: use of negative muons at riken-ral port4 for elemental characterization of "nuragic votive ship" samples. *Nucl. Instrum. Methods Phys. Res. Sect. A Accel. Spectrom. Detect. Assoc. Equip.* 936, 27–28. doi:10.1016/j.nima.2018.11.076

Dal Maso, G., Barchetti, F., Francesconi, M., Galli, L., Greuter, U., Hildebrandt, M., et al. (2023). Beam monitoring detectors for high intensity muon beams. *Nucl. Instrum. Methods Phys. Res. Sect. A Accel. Spectrom. Detect. Assoc. Equip.* 1047, 167739. doi:10.1016/j.nima.2022.167739

Hillier, A. D., Lord, J. S., Ishida, K., and Rogers, C. (2019). Muons at isis. *Philosophical Trans. R. Soc. A Math. Phys. Eng. Sci.* 377, 20180064. doi:10.1098/rsta.2018.0064

Lord, J., McKenzie, I., Baker, P., Blundell, S. J., Cottrell, S. P., Giblin, S. R., et al. (2011). Design and commissioning of a high magnetic field muon spin relaxation spectrometer at the isis pulsed neutron and muon source. *Rev. Sci. Instrum.* 82, 073904. doi:10.1063/1.3608114

Matsuzaki, T., Ishida, K., Nagamine, K., Watanabe, I., Eaton, G., and Williams, W. (2001). The riken-ral pulsed muon facility. *Nucl. Instrum. Methods Phys. Res. Sect. A Accel. Spectrom. Detect. Assoc. Equip.* 465, 365–383. doi:10.1016/S0168-9002(01)00694-5

Papa, A., Barchetti, F., Gray, F., Ripiccini, E., and Rutar, G. (2015). A multi-purposed detector with silicon photomultiplier readout of scintillating fibers. *Nucl. Instrum. Methods Phys. Res. Sect. A Accel. Spectrom. Detect. Assoc. Equip.* 787, 130–133. doi:10.1016/j.nima.2014.11.074

Papa, A., Rutar, G., Barchetti, F., Hildebrandt, M., and Kettle, P. (2019). A fast and quasi non-invasive muon beam monitor working at the intensity frontier. *Nucl. Instrum. Methods Phys. Res. Sect. A Accel. Spectrom. Detect. Assoc. Equip.* 936, 634–635. doi:10.1016/j.nima.2018.10.145

Pizzolotto, C., Adamczak, A., Bakalov, F. D., et al. (2020). The famu experiment: muonic hydrogen high precision spectroscopy studies. *Eur. Phys. J.* A 56, 185. doi:10.1140/epja/s10050-020-00195-9

Rossini, R., Adamczak, A., Bakalov, D., Baldazzi, G., Banfi, S., Baruzzo, M., et al. (2024a). Status of the detector setup for the famu experiment at riken-ral for a precision measurement of the zemach radius of the proton in muonic hydrogen. *J. Instrum. (JINST)* 19, C02034. doi:10.1088/1748-0221/19/02/C02034

Rossini, R., Benocci, R., Bertoni, R., Bonesini, M., Carsi, S., Clemenza, M., et al. (2024b). Characterisation of a low-momentum high-rate muon beam monitor for the famu experiment at the cnao-xpr beam facility. *J. Instrum. (JINST)* 19, C01024. doi:10.1088/1748-0221/19/01/C01024

Rossini, R., Benocci, R., Bertoni, R., Bonesini, M., Clemenza, M., De Vecchi, C., et al. (2023a). Characterisation of a scintillating fibre-based hodoscope exposed to the cnao low-energy proton beam. *Nucl. Instrum. Methods Phys. Res. Sect. A Accel. Spectrom. Detect. Assoc. Equip.* 1046, 167746. doi:10.1016/j.nima.2022.167746

Rossini, R., Benocci, R., Bertoni, R., Bonesini, M., Clemenza, M., Menegolli, A., et al. (2023b). Characterisation of muon and proton beam monitors based on scintillating fibres with a sipm read-out. *Nucl. Instrum. Methods Phys. Res. Sect. A Accel. Spectrom. Detect. Assoc. Equip.* 1046, 167684. doi:10.1016/j.nima.2022.167684

Rossini, R., Di Martino, D., Agoro, T., Cataldo, M., Gorini, G., Hillier, A. D., et al. (2023c). A new multidisciplinary non-destructive protocol for the analysis of stony meteorites: gamma spectroscopy, neutron and muon techniques supported by Raman microscopy and sem-eds. *J. Anal. At. Spectrom.* 38, 293–302. doi:10.1039/D2JA00263A

Vacchi, A., Mocchiutti, E., Adamczak, A., Bakalov, D., Baldazzi, G., Baruzzo, M., et al. (2023). Investigating the proton structure: the famu experiment. *Nucl. Phys. News* 33, 9–16. doi:10.1080/10619127.2023.21989132198913

Vlachoudis, V. (2009). "Flair: a powerful but user friendly graphical interface for FLUKA," in International Conference on Mathematics, Computational Methods & Reactor Physics 2009, Saratoga Springs, New York, 3-7 May 2009, 790–800.